

Atom Exchange between Aqueous Fe(II) and Goethite: An Fe Isotope Tracer Study

ROBERT M. HANDLER,[†]
BRIAN L. BEARD,[‡] CLARK M. JOHNSON,[‡]
AND MICHELLE M. SCHERER*[†]

Department of Civil and Environmental Engineering,
University of Iowa, 4105 Seamans Center, Iowa City, Iowa
52242, and Department of Geology and Geophysics, University
of Wisconsin, Madison, 1215 West Dayton Street, Madison,
Wisconsin 53706

Received August 27, 2008. Revised manuscript received
November 27, 2008. Accepted December 10, 2008.

The reaction of aqueous Fe(II) with Fe(III) oxides is a complex process, comprising sorption, electron transfer, and in some cases, reductive dissolution and transformation to secondary minerals. To better understand the dynamics of these reactions, we measured the extent and rate of Fe isotope exchange between aqueous Fe(II) and goethite using a ⁵⁷Fe isotope tracer approach. We observed near-complete exchange of Fe atoms between the aqueous phase and goethite nanorods over a 30-day time period. Despite direct isotopic evidence for extensive mixing between the aqueous and goethite Fe, no phase transformation was observed, nor did the size or shape of the goethite rods change appreciably. High-resolution transmission electron microscopy images, however, appear to indicate that some recrystallization of the goethite particles may have occurred. Near-complete exchange of Fe between aqueous Fe(II) and goethite, coupled with negligible change in the goethite mineralogy and morphology, suggests a mechanism of coupled growth (via sorption and electron transfer) and dissolution at separate crystallographic goethite sites. We propose that sorption and dissolution sites are linked via conduction through the bulk crystal, as was recently demonstrated for hematite. Extensive mixing between aqueous Fe(II) and goethite, a relatively stable iron oxide, has significant implications for heavy metal sequestration and release (e.g., arsenic and uranium), as well as reduction of soil and groundwater contaminants.

Introduction

The redox reactions of iron (Fe) influence a variety of global elemental cycles such as carbon and nitrogen through Fe-limited primary production (1). Redox transitions between soluble Fe(II) and solid Fe(III) phases are also suspected to play an important role in mobilization and transformation of a variety of trace heavy metals such as arsenic and lead (2, 3). A better understanding of these Fe redox processes is critical to our ability to predict and influence biogeochemical cycling of elements on global and local levels.

Microbial respiration of Fe(III) oxides results in significant quantities of reduced, soluble Fe(II) in subsurface environments (4). Reaction between aqueous Fe(II) and Fe(III) oxides has been studied extensively, and these studies have revealed that the reaction is more complex than sorption alone. Experiments investigating reactions of Fe(II) with Fe oxides have often relied on solution phase measurements of Fe(II) after exposure to Fe oxides, attributing the loss of Fe(II) from solution to sorption. In some cases, Fe(II) lost from solution has not been completely recovered after lowering the solution pH (e.g., ref 5), which has been interpreted as possible incorporation of Fe(II) within the Fe oxide surface structure or oxidation to Fe(III) (6, 7). We, as well as others, have used ⁵⁷Fe Mössbauer spectroscopy to show that after sorption, electron transfer occurs between sorbed Fe(II) and the Fe(III) oxide, forming an oxidized Fe surface layer (8–11). Pedersen et al. used ⁵⁵Fe-labeled synthetic Fe oxides to show that aqueous Fe(II) can also catalyze reductive dissolution of Fe atoms originally bound within an Fe oxide (12). For the more unstable Fe(III) oxides, such as ferrihydrite and lepidocrocite, secondary mineralization to more stable Fe oxides such as goethite or magnetite has been observed (12–15). Although sorption of Fe(II) to goethite and hematite occurs over a wide range of pH values (5, 16), and interfacial electron transfer has been demonstrated on these oxides (10, 17), no phase transformations have been observed, and little to no reductive dissolution of Fe(II) occurs after reaction of Fe(II) with goethite or hematite, respectively (12). This leaves us with an unclear picture of the nature and extent of the reaction of Fe(II) with goethite, one of the most prevalent environmental Fe oxide phases.

A promising method for investigating the redox cycling of Fe involves selective use of Fe isotopes. There are four stable isotopes of Fe that differ widely in their natural abundance: ⁵⁴Fe (5.8%), ⁵⁶Fe (91.8%), ⁵⁷Fe (2.1%), and ⁵⁸Fe (0.3%) (18). Recent advancements in mass spectrometry (multicollector inductively coupled plasma mass spectrometry or MC-ICP-MS) allow us to distinguish between isotopes of heavy elements such as Fe with great precision (19). Stable isotope studies have been recently used to assess which biogeochemical processes might cause the variations in Fe isotope composition observed in nature (20–23). For example, there have been several Fe isotope studies of Fe isotope fractionation caused by the interaction of aqueous Fe(II) with iron oxides. Icopini et al. (24) and Teutsch et al. (25) inferred that sorption of Fe(II) onto the iron oxide is an important process in controlling the Fe isotope composition of aqueous Fe, although these studies did not directly measure the sorbed Fe(II). Recent studies by Crosby and co-workers have shown that although sorption of Fe(II) onto iron oxides produces a measurable Fe isotope fractionation, the most significant control on the Fe isotope composition of aqueous Fe(II) is electron and isotope exchange with a reactive Fe(III) layer on the iron oxide substrate (20, 26).

In this study, we used a ⁵⁷Fe-enriched tracer to investigate atom exchange between aqueous Fe(II) and goethite. Importantly, the Fe isotope variations associated with this tracer approach are over 100 times greater than the mass-dependent Fe isotope fractionations that have been previously identified, allowing unambiguous identification of Fe isotope exchange. The approach used in this study is similar to that followed by Skulan et al. (27), Poulson et al. (28), Welch et al. (29), and Shahar et al. (30) to identify isotope exchange between aqueous Fe(III) and hematite, aqueous Fe(III) and ferrihydrite, aqueous Fe(III) and Fe(II), and magnetite and fayalite, respectively. Here, we react aqueous Fe(II) enriched in ⁵⁷Fe

* Corresponding author phone: (319) 335-5654; fax: (319) 335-5660; e-mail: michelle-scherer@uiowa.edu.

[†] University of Iowa.

[‡] University of Wisconsin.

with goethite rods to identify isotope exchange between aqueous Fe(II) and goethite. We demonstrate that, despite no obvious physical change in the goethite rods, the Fe isotopes become evenly dispersed between the aqueous phase and the solid Fe(III) lattice, which implies that near-complete mixing of Fe atoms has occurred.

Experimental Section

Goethite Synthesis and Characterization. The goethite solids used here are the same nanorod particles we synthesized and characterized in our previous work (17). Goethite rods had an average length and width of 81 ± 28 and 11 ± 4 nm, respectively, and a specific surface area of $110 (\pm 7) \text{ m}^2/\text{g}$ (17). X-ray diffraction (XRD) patterns and Mössbauer spectra were consistent with goethite (data not shown).

Solids were characterized after mixing with or without aqueous Fe(II). XRD samples were prepared by combining filtered solids with a small amount of glycerol to create an oxide slurry to prevent oxidation of Fe(II). Transmission electron microscopy (TEM) samples were prepared by rinsing filtered solids with a small amount of deionized water ($> 18 \text{ M}\Omega \cdot \text{cm}$) to remove buffer salts and aqueous Fe(II), then resuspending the solids in deionized water before placement on a carbon-coated Cu grid. High-resolution TEM (HR-TEM) samples were prepared to examine variations in the crystal structure of goethite particles after exposure to Fe(II). HR-TEM samples were rinsed and suspended in DI water, then resuspended in methanol to reduce particle aggregation before placement on a holey carbon grid. High-resolution images were taken on a JEOL 2100-F electron microscope.

^{57}Fe (II) Isotope Tracer Experiment. All experiments were carried out in an anoxic glovebox, with care taken to prevent O_2 intrusion into the reactors during centrifugation outside of the anoxic environment. All chemicals were reagent grade, and solutions were made in deionized water. HCl acid used in experimental procedures was purified by sub-boiling distillation. A ^{57}Fe -enriched aqueous Fe(II) stock was prepared in 0.5 M HCl by dissolving enriched ^{57}Fe (Chemgas, 96% ^{57}Fe) and adding a small amount to an isotopically normal Fe(II) stock to provide an $\sim 80\%$ increase in $^{57}\text{Fe}/^{56}\text{Fe}$ ratio relative to “normal” Fe. Use of enriched ^{57}Fe does not affect the rate of exchange as demonstrated by similar rates of exchange measured for Fe(II)(aq)–Fe(III)(aq) using both ^{55}Fe and ^{59}Fe (31, 32), nor does use of enriched isotopic tracers affect the approach to isotopic equilibrium because there is no evidence for changes in mechanism as a function of mass.

Batch reactors were prepared by adding 15 mL of pH 7.5 HEPES buffer (25 mM HEPES plus 25 mM KBr electrolyte) to a 20 mL glass vial and adding Fe(II) stock to reach an initial Fe(II) concentration of ~ 1 mM. Vials were counter-spiked with 0.5 M KOH prior to Fe(II) addition in order to keep the pH stable at 7.5. After 1 h of equilibration, the Fe(II)–HEPES solution was filtered through a $0.2 \mu\text{m}$ filter into a 30 mL Nalgene centrifuge tube and the Fe(II) concentration was measured. Goethite solids were added to the reactors in preweighed 30 mg portions (solids loading 2 g/L), which were placed on an end-over-end rotator and allowed to mix in the dark for times ranging from 10 min to 30 days. The solution pH did not deviate more than ± 0.1 for the duration of the experiment. Control reactors were included with aqueous Fe(II) alone and goethite alone.

Three reactors were sacrificed at each time point for isotopic and chemical analyses. After centrifugation at 30 000g, the reactor supernatant was decanted, filtered into a new vial, and acidified for aqueous Fe(II) and total Fe analyses. Remaining goethite solids in the reactor were resuspended for 10 min with 5 mL of 0.4 M HCl to remove solid-associated Fe(II). After centrifugation and removal of the 0.4 M HCl supernatant, two successive acid extractions of the remaining solids were performed (5 mL of 1 M HCl,

45 min at 60°C) to remove any remaining Fe(II) and dissolve a small portion ($\sim 5\%$) of the Fe(III) within the goethite. The remaining bulk solids were completely dissolved in 5 M HCl. Here, we report only on the results for aqueous Fe(II) and Fe(III) from the remaining bulk solids.

Chemical Fe Analyses. Fe(II) concentrations were measured for aqueous and acid-dissolved Fe extractions using the 1,10-phenanthroline method with fluoride added to remove interference from aqueous Fe(III) (33). Fe(III) content in each extraction was determined by the difference between measured Fe(II) concentrations and total Fe content, which was obtained through addition of hydroxylamine hydrochloride reductant to separate Fe analysis samples.

Fe Isotope Analyses. Prior to isotopic analysis, all Fe samples were oxidized with hydrogen peroxide. Samples were purified using anion-exchange chromatography (Fe yields from ion-exchange columns were $> 95\%$), and Fe isotopes were analyzed using a Micromass IsoProbe, a single-focusing MC-ICP–MS, following the methods of Beard et al. (19), except we did not use desolvation nebulization in order to allow for rapid washout between solutions that differed by up to 80% in their Fe isotope compositions. Instead, solutions (3 ppm) were aspirated at $100 \mu\text{L}/\text{min}$ using a concentric flow nebulizer and a cyclonic spray chamber that was cooled to 5°C . We report Fe isotope compositions in δ notation, which has the form

$$\delta^{57/56}\text{Fe} (\text{‰}) = \left(\frac{\frac{^{57}\text{Fe}}{^{56}\text{Fe}}_{\text{sample}} - \frac{^{57}\text{Fe}}{^{56}\text{Fe}}_{\text{std}}}{\frac{^{57}\text{Fe}}{^{56}\text{Fe}}_{\text{std}}}} \right) \times 1000 \quad (1)$$

where $^{57}\text{Fe}/^{56}\text{Fe}_{\text{std}}$ is the average isotopic ratio for bulk igneous rocks (21). On the basis of replicate analyses of 33 samples passed through the entire analytical process, the average one standard deviation is 0.13‰ in $^{57}\text{Fe}/^{56}\text{Fe}$. Analytical uncertainties are slightly higher using the cyclonic spray chamber, as compared to using desolvation nebulization. During the course of this study the measured $\delta^{57/56}\text{Fe}$ value of the IRMM-014 standard was $-0.03\text{‰} \pm 0.05\text{‰}$ (1 SD; $n = 4$). Accuracy of Fe isotope results was checked by nine analyses of synthetic samples that contained 0.5 mM Fe of known Fe isotope composition in the same matrix as the aqueous Fe samples. These synthetic samples were processed in the same fashion as the Fe samples, and the measured $\delta^{57/56}\text{Fe}$ value of these synthetic samples ($+0.38\text{‰} \pm 0.08\text{‰}$) exactly matched the Fe isotope composition of the pure Fe standard ($+0.37\text{‰} \pm 0.09\text{‰}$, $n = 25$), demonstrating that our analytical technique is free of matrix effects. Partial acid digestion of goethite crystals demonstrated that the goethite used in the experiments is not isotopically zoned; the $\delta^{57/56}\text{Fe}$ of a 6% partial dissolution of goethite is -0.04‰ , which is analytically indistinguishable from the $\delta^{57/56}\text{Fe}$ value of the remaining residue, -0.16‰ .

Results and Discussion

We used Fe isotopes to track the movement of Fe between the aqueous phase and goethite during a batch Fe(II) sorption experiment. Aqueous Fe(II) was enriched with ^{57}Fe to give distinctly different isotopic compositions for the aqueous Fe(II) and Fe(III) within the goethite structure (Figure S1 in the Supporting Information). The enriched aqueous Fe(II) contained roughly twice as many ^{57}Fe atoms as would be expected in nature ($\delta^{57/56}\text{Fe} = +840.43\text{‰}$). Goethite rods were not enriched and had an initial $\delta^{57/56}\text{Fe}$ value of -0.12‰ . Enriching the aqueous Fe(II) with ^{57}Fe allowed us to track the movement of Fe atoms between the aqueous phase and solid phase by measuring the $\delta^{57/56}\text{Fe}$ of each phase over

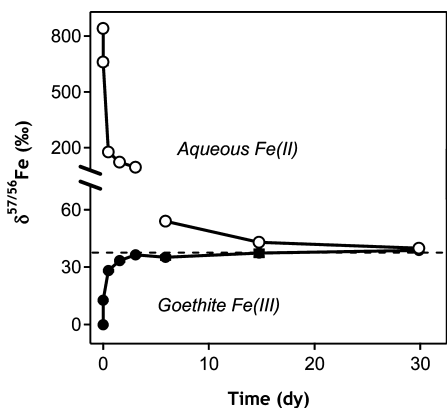


FIGURE 1. Measured $\delta^{57/56}$ values of aqueous Fe(II) and residual goethite over time. Dashed line represents the completely mixed $\delta^{57/56}$ Fe value of 37.57‰ calculated from eq 2 in the text (i.e., $\delta^{57/56}\text{Fe}_{\text{sys}} = (15.85 \times 840.43 + 337.66 \times -0.12)/(15.85 + 337.66) = 37.57$). Each data point represents the average of triplicate reactors. Standard deviations of replicates are contained within markers.

time with MC-ICP-MS. The same kinetic results would be obtained if isotopically normal Fe(II) and ^{57}Fe -enriched goethite were used (e.g., ref 27).

Over the course of 30 days, the $\delta^{57/56}\text{Fe}$ values of aqueous Fe(II) decreased from +840.43‰ to +39.94‰, indicating that some of the ^{57}Fe -enriched aqueous Fe had been replaced with ^{56}Fe atoms (Figure 1). The $\delta^{57/56}\text{Fe}$ values of the goethite solids rose sharply from -0.12‰ to +38.75‰, implying that isotopic exchange had occurred and the content of ^{57}Fe relative to ^{56}Fe had increased in the goethite solids. By the end of the experiment, the aqueous and goethite Fe reservoirs reached similar isotopic compositions of +39.94‰ \pm 1.16‰ and +38.75‰ \pm 0.72‰, respectively (\pm 1 SD), demonstrating that significant mixing occurred between the two reservoirs. No significant changes in $\delta^{57/56}\text{Fe}$ values of control reactors (goethite alone or aqueous Fe(II) alone) were detected (data not shown).

To evaluate the extent of mixing, we calculated a mass-balance-weighted isotopic composition of the two-component system using

$$(\delta^{57/56}\text{Fe}_{\text{sys}})[\text{Fe}_{\text{goethite}} + \text{Fe}_{\text{spike}}] = (\delta^{57/56}\text{Fe}_{\text{goethite}})[\text{Fe}_{\text{goethite}}] + (\delta^{57/56}\text{Fe}_{\text{spike}})[\text{Fe}_{\text{spike}}] \quad (2)$$

where $\delta^{57/56}\text{Fe}$ and $[\text{Fe}]$ refer to the $^{57}\text{Fe}/^{56}\text{Fe}$ ratio in δ notation and molar amounts of the initial goethite and Fe(II) spike given in the first row of Table 1. If complete mixing occurred between the Fe atoms in goethite and the aqueous Fe(II) atoms, the homogenized Fe suspension would have a $\delta^{57/56}\text{Fe}_{\text{sys}}$ of +37.57‰ \pm 1.15‰ (dashed line in Figure 1). The aqueous and goethite Fe(III) $\delta^{57/56}\text{Fe}$ values of +39.94‰ and +38.75‰ measured at the end of the experiment are remarkably close to the $\delta^{57/56}\text{Fe}_{\text{sys}}$ of +37.57‰ calculated for the completely mixed isotopic composition and indicate that greater than 95% exchange occurred. Convergence of the aqueous and goethite $\delta^{57/56}\text{Fe}$ values to the calculated value for complete mixing demonstrates that the Fe atoms in the aqueous phase and goethite solids have become nearly completely mixed over a period of 30 days.

Previous work has also provided evidence that atom exchange between Fe(III) oxides and aqueous Fe(II) occurs. Pedersen et al. incorporated ^{55}Fe into several different Fe oxides and observed the release of ^{55}Fe into solution upon exposure to aqueous Fe(II) (12). Release of ^{55}Fe into solution was observed for lepidocrocite, ferrihydrite, and goethite, but not for hematite. With lepidocrocite and ferrihydrite, the amount of ^{55}Fe released into solution approached isotopic

equilibrium and was accompanied by significant phase transformation. For goethite, however, they observed much less exchange with only 5–10% of the goethite atoms released into solution after 16 days and no apparent phase transformation. Here, we observed significantly more atom exchange with most of the goethite atoms exchanged after 30 days. Relative to the experimental conditions of Pedersen et al., our goethite particles have a greater surface area (110 vs 37 m²/g), and we worked at a higher solution pH (7.5 vs 6.5) and higher solids loading (2 g/L vs ~50 mg/L). These differences, as well as other experimental variables, such as pH buffer and background electrolyte, may have contributed to the differences in amount of Fe exchanged in the two goethite experiments. Despite differences in the extent of Fe atom exchange, both the isotope data here and the ^{55}Fe release observed by Pedersen et al. provide compelling evidence that significant atom exchange occurs between goethite and aqueous Fe(II).

Recent work by Jang et al. (23) has also investigated the interaction between Fe(II) and goethite using natural Fe isotope abundances. $\delta^{56/54}\text{Fe}$ values were measured for aqueous Fe(II), as well as 0.5 M HCl-extractable Fe(II) using solution conditions analogous to those used here. On the basis of a mass-balance estimate, the authors concluded that isotope mixing between Fe(II) and goethite Fe(III) atoms occurs. Here, by using ^{57}Fe as a tracer in the aqueous phase, we were able to simultaneously track the aqueous and solid phase isotope ratios and demonstrate, by direct measurements, that atom exchange between Fe(II) and goethite does indeed occur and that it is extensive enough to reach isotopic equilibrium.

Despite the extensive Fe exchange observed in our isotope tracer experiment, the aqueous Fe(II) concentration remained relatively stable after initial Fe(II) uptake. Within minutes, the aqueous Fe(II) concentration decreased from 1.07 to 0.55 mM and remained relatively constant over the remaining 30 days (Table 1 and Figure S2, Supporting Information). A similar amount and rate of Fe(II) sorption was observed in our previous work with these particles resulting in an estimated surface coverage well below monolayer (i.e., about 30% assuming four sites/nm² and an idealized goethite geometry) (17). We do not see any evidence of the slower, gradual decrease following an initial rapid uptake that has been reported by several others and attributed to a transition between outer-sphere and inner-sphere adsorption or the formation of surface-associated Fe(II) structures (7, 16, 34). The average Fe(II) recovery over our entire experimental procedure was >96% (calculated from the total of Fe(II) recoveries in each of the five sample extractions), indicating that losses of Fe(II) throughout the sampling procedures and acid extractions were minimal. Our observation that aqueous Fe(II) concentrations were relatively stable despite significant changes in the $\delta^{57/56}\text{Fe}$ values suggests that the system was at steady-state conditions and that isotopic exchange occurred without significant net dissolution or precipitation occurring beyond the initial Fe(II) loss from solution.

In the solid phase, negligible change was observed in the mineralogy, shape, or size of the goethite particles before and after reaction with Fe(II). XRD patterns revealed no formation of secondary mineral phases and negligible increases in average crystallite size via the Scherrer equation (Figure S3, Supporting Information). Lattice spacings from HR-TEM images are also consistent with goethite confirming that there was no significant formation of a secondary mineral phase (Figure S4, Supporting Information). TEM images revealed little change in the size and shape of the goethite particles when exposed to 1 mM Fe(II) (Figure S5, Supporting Information). A more quantitative assessment of the particle size distribution on the TEM images shows no change in the length (81 \pm 28 to 82 \pm 32 nm) or width (11 \pm 4 to 11 \pm 5

TABLE 1. Chemical and Isotopic Data during Enriched Fe Isotope Tracer Experiment

time	aqueous Fe(II)			goethite ^a	
	Fe(II) _{aq} mM	Fe(II) _{aq} μmol	δ ^{57/56} Fe (‰)	Fe(III) _s μmol	δ ^{57/56} Fe (‰)
0	1.07 (0.03) ^b	15.85 (0.46)	840.43 (0.18)	337.66 (3.4) ^c	-0.12 (0.02)
10 min	0.55 (0.01)	8.17 (0.17)	660.64 (13.21)	332.96 (17.99)	12.71 (0.16)
12 h	0.52 (0.00)	7.70 (0.06)	176.95 (10.60)	278.27 (8.37)	28.25 (0.19)
1.6 days	0.57 (0.01)	8.48 (0.12)	122.36 (2.50)	263.82 (8.47)	33.36 (0.26)
3.1 days	0.62 (0.01) ^d	9.14 (0.13)	94.72 (8.22)	275.24 (4.54)	36.47 (0.32)
5.9 days	0.54 (0.01)	8.02 (0.17)	54.00 (1.81)	301.88 (4.43)	35.13 (0.90)
14.8 days	0.52 (0.04)	7.78 (0.61)	43.01 (1.87)	297.35 (13.84)	37.38 (1.70)
30 days	0.54 (0.01)	8.05 (0.14)	39.94 (1.16)	309.30 (15.01)	38.75 (0.72)

^a Goethite measurements were collected on all remaining solids at the end of the sequential extraction procedure by completely dissolving solids in 5 M HCl at 60 °C. ^b Numbers in parentheses represent one standard deviation based on triplicate reactors; this standard deviation does not reflect the analytical uncertainty of an Fe isotope measurement but rather the consistency of the entire experiment. The analytical uncertainty of a single δ^{57/56}Fe measurement is ± 0.13‰ based on replicate analysis of samples and standards, as reported in the text. ^c Differences in Fe(III)_s recoveries are due to varying losses of goethite solids during decanting and filtration steps prior to complete dissolution of the remaining bulk goethite. ^d Samples sacrificed after *t* = 3.1 days were inadvertently spiked with a slightly higher initial Fe(II) concentration, hence the slightly higher aqueous Fe(II) concentration of 0.62 mM.

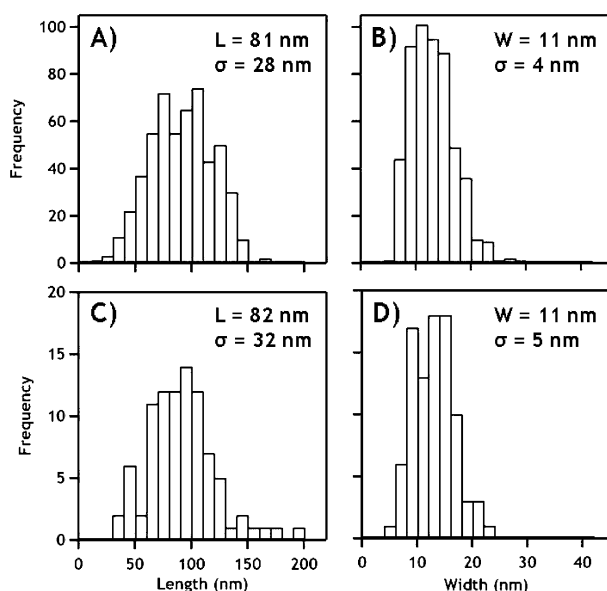


FIGURE 2. Particle size distributions for length and width of goethite particles before (A and B) and after reaction with Fe(II) (C and D). More particles were included in the analysis for untreated goethite rods than for goethite reacted with Fe(II) (*n* = 530 vs *n* = 91), resulting in greater frequency numbers in panels A and B. Average particle lengths or widths and one standard deviations are shown in the panels.

nm) of the goethite (Figure 2). Interestingly though, HR-TEM images suggest that some changes to the goethite particles may have occurred during Fe isotope exchange (Figure S4, Supporting Information). After reaction with Fe(II) for 30 days, the rods appear to have become more crystalline. The potential for recrystallization after reaction with Fe(II) is an avenue we are currently exploring with additional HR-TEM work.

How such extensive Fe atom exchange can occur, as required by the isotopic data, with no significant morphological change is a fascinating question. Diffusion of Fe through the solid goethite structure is one potential explanation. Solid-state diffusion rates have been measured for Fe atoms in various solid Fe phases (35–37), but generally these studies are performed at temperatures ranging from ~700–1500 °C in order to generate Fe diffusion rates that are measurable on reasonable experimental time scales. Even if Fe atom diffusion were to occur solely along crystallite

grain boundaries or defect sites, estimates of diffusion time of Fe at room temperature would exceed millions of years to move just a few nanometers through an Fe oxide lattice.

Although we can eliminate solid-state diffusion as a reasonable explanation for Fe isotope exchange, we cannot rule out the possibility of diffusion through micropores in the goethite structure. Diffusion through micropores has often been invoked to explain the gradual loss of ions from solution in the presence of iron oxides (38, 39). Recently, long-term rates of loss of a variety of metal cations (not Fe) from solution in the presence of goethite have been correlated with ionic radius, which has been interpreted as evidence for a micropore diffusion mechanism governing incorporation of these ions into goethite (40). Here, however, we see a stable aqueous Fe(II) concentration after the initial Fe(II) sorption, which suggests that gradual diffusion into goethite micropores is not a likely explanation for the Fe atom exchange we observe here.

Another potential mechanism to explain how all the Fe goethite atoms have become mixed with the Fe atoms in solution is coupling electron conduction through the bulk goethite with growth and dissolution. Yanina and Rosso recently demonstrated that a potential gradient can be measured between different crystal faces on hematite and that conduction through the bulk oxide can result in growth and dissolution at separate crystal faces (41). We propose that a similar mechanism may be associated with Fe(II)–goethite exchange.

From our previous studies utilizing Mössbauer spectroscopy, we know that sorption of Fe(II) onto goethite results in electron transfer between the sorbed Fe(II) and the structural Fe(III) in goethite (8, 9). We also know that oxidation of the sorbed Fe(II) results in growth of goethite on goethite (i.e., homoepitaxy) (8), as well as injection of an electron into the goethite structure. We do not know the exact fate of the electron, but from the ⁵⁵Fe dissolution and stable isotope work of others (12, 23), and our isotope data here, it is clear that some of the bulk Fe(III) goethite is reduced and released into solution. If the electron was transferred from sorbed Fe(II) through the Fe lattice by bulk conduction across a potential gradient, the goethite Fe(III) atom could be dissolving at a different location on the goethite surface. These newly reduced Fe(III) atoms, now Fe(II), could then dissolve into the aqueous phase, exposing fresh Fe(III) atoms in goethite to the aqueous phase. Through a repeated series of these five steps of sorption–electron transfer–crystal growth–conduction–dissolution, a redox-driven conveyor belt could be established that would allow all of the goethite

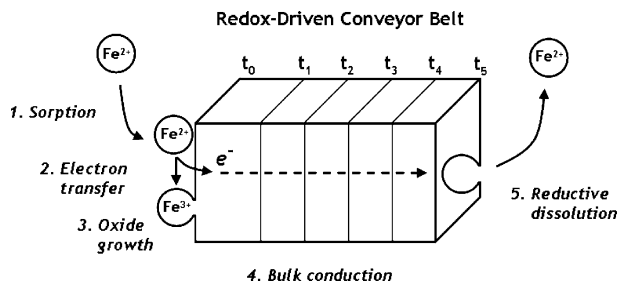


FIGURE 3. Conceptual model for the five steps associated with the redox-driven conveyor belt mechanism to explain how bulk goethite Fe(III) atoms and aqueous Fe(II) can become completely mixed via growth and dissolution at separate goethite surface sites. The left surface may be considered a reference plane in the original goethite crystal at the start of the process (t_0), and through growth on the left and dissolution on the right, this reference plane will migrate over time ($t_0 \rightarrow t_5$) until time t_5 , at which point 100% atom exchange has occurred.

to be eventually exposed to the aqueous phase and exchanged (Figure 3). This surface-mediated exchange process would result in similar Fe isotope distributions in the aqueous phase and goethite particle as we have observed here. This mechanism is also consistent with a stable aqueous Fe(II) concentration if there were equal rates of goethite growth and dissolution, that is, no net growth and dissolution beyond the initial Fe(II) uptake.

At this point, however, it is unclear if electron transport rates are fast enough in goethite for the conveyor belt model to explain the extensive atom exchange we observed over a few weeks. For electron transport to occur through the bulk goethite, a potential gradient needs to exist between different crystal sites and the goethite has to be sufficiently conductive. Goethite is about 10-fold less conductive than hematite (42). The limitations imposed by lower conductivity, however, are compensated by the much shorter electron transport paths for the goethite rods (<100 nm) compared to the hematite single crystal (1 mm) used by Yanina and Rosso (41). It therefore seems reasonable that the goethite nanorods could be sufficiently conductive at the nanometer scale to support a conveyor belt mechanism.

Because we see no net change in crystal shape of the goethite particles, it is more difficult to argue that a potential gradient exists between different crystal faces. Our analysis, however, is based on average length and width values obtained from TEM images. We could be missing subtler changes in the crystals, such as changes in crystal faces that parallel the *c*-axis or changes in the step density or surface roughness. There is some evidence that both of these changes occur on goethite particles in the presence of Fe(II). For example, a difference in growth rates for the (100) and (110) faces of goethite was reported when Fe(II) was oxidized by Oxygen, suggesting different reactivity for the (100) and (110) faces, which both run parallel to the *c*-axis (43). Chun et al. also observed preferred oxidation of Fe(II) and reduction of an organic contaminant at a specific crystal face, leading to growth along the *c*-axis and increased roughness of the goethite particle tips (44).

The environmental implications of complete atom exchange between Fe(II) and goethite observed are significant. Goethite and other stable Fe oxides are considered major sources and sinks of trace heavy metals, and formation and dissolution of Fe oxides can control metal availability in natural and engineered systems (45, 46). We have demonstrated here that despite an apparent phase stability in Fe(II)–goethite suspensions, there is actually a tremendous amount of Fe atom cycling occurring between the aqueous and solid phases. In the presence of aqueous Fe(II), heavy

metals thought to be sequestered in bulk Fe oxides may actually become available on the particle surface or in the aqueous phase as a result of this exchange. Conversely, a larger than expected uptake of metals from the aqueous phase could occur as a result of the continuous reformation of the Fe oxide structure, exposing the entire crystal for equilibration and sequestration of metals, rather than just the surface sites or porous cavities. Indeed, previous work has demonstrated that the addition of minute quantities of Fe(II) to a goethite suspension can induce measurable increases in sorption of other metal cations, despite the prevailing assumption that the Fe(II) would merely compete for goethite surface sites (6). The implications of such significant mixing between aqueous Fe(II) and Fe(III) oxides require further investigation, and subsequent predictive and modeling efforts should consider the effects of Fe exchange in the presence of aqueous Fe(II).

Acknowledgments

This work was supported by a National Science Foundation NIRT Grant (EAR-0506679). We thank A. Heimann, A. Czaja, L. Wu, and S. Ready at UW-Madison for assisting with sample preparation, and D. Latta and C. Gorski at the University of Iowa for helpful discussions regarding the manuscript. We also thank J. Baltrusaitis of the Central Microscopy Research Facility at The University of Iowa for collecting the HR-TEM images at Northwestern University. The manuscript was greatly improved with the help of three anonymous reviewers.

Supporting Information Available

Figures displaying initial conditions for the isotope tracer study, aqueous Fe(II) concentration in experimental reactors over time, XRD patterns of goethite particles mixed with or without exposure to aqueous Fe(II), HR-TEM and TEM images of goethite particles with and without Fe(II) exposure. This material is available free of charge via the Internet at <http://pubs.acs.org>.

Literature Cited

- Jickells, T. D.; An, Z. S.; Andersen, K. K.; Baker, A. R.; Bergametti, G.; Brooks, N.; Cao, J. J.; Boyd, P. W.; Duce, R. A.; Hunter, K. A.; Kawahata, H.; Kubilay, N.; laRoche, J.; Liss, P. S.; Mahowald, N.; Prospero, J. M.; Ridgwell, J.; Tegen, I.; Torres, R. Global iron connections between desert dust, ocean biogeochemistry, and climate. *Science* **2005**, *308*, 67–71.
- Dixit, S.; Hering, J. G. Comparison of arsenic (V) and arsenic (III) sorption onto iron oxide minerals: Implications for arsenic mobility. *Environ. Sci. Technol.* **2003**, *37*, 4182–4189.
- Dong, D. M.; Nelson, Y. M.; Lion, L. W.; Shuler, M. L.; Ghiorse, W. C. Adsorption of Pb and Cd onto metal oxides and organic material in natural surface coatings as determined by selective extractions: new evidence for the importance of Mn and Fe oxides. *Water Res.* **2000**, *34*, 427–436.
- Chapelle, F. H.; Lovley, D. R. Competitive exclusion of sulfate reduction by Fe(III)-reducing bacteria: A mechanism for producing discrete zones of high-iron ground water. *Ground Water* **1992**, *30*, 29–36.
- Jeon, B. H.; Dempsey, B. A.; Burgos, W. D.; Royer, R. A. Reactions of ferrous iron with hematite. *Colloids Surf., A* **2001**, *191*, 41–55.
- Coughlin, B. R.; Stone, A. T. Nonreversible adsorption of divalent metal-ions (Mn(II), Co(II), Ni(II), Cu(II), and Pb(II)) onto goethite—effects of acidification, Fe(II) addition, and picolinic-acid addition. *Environ. Sci. Technol.* **1995**, *29*, 2445–2455.
- Jeon, B. H.; Dempsey, B. A.; Burgos, W. D. Kinetics and mechanisms for reactions of Fe(II) with iron(III) oxides. *Environ. Sci. Technol.* **2003**, *37*, 3309–3315.
- Williams, A. G. B.; Scherer, M. M. Spectroscopic evidence for Fe(II)–Fe(III) electron transfer at the Fe oxide–water interface. *Environ. Sci. Technol.* **2004**, *38*, 4782–4790.
- Silvester, E.; Charlet, L.; Tournassat, C.; Gehin, A.; Grenèche, J. M.; Liger, E. Redox potential measurements and Mossbauer spectrometry of Fe(II) adsorbed onto Fe(III) (oxyhydr)oxides. *Geochim. Cosmochim. Acta* **2005**, *69*, 4801–4815.

- (10) Larese-Casanova, P.; Scherer, M. M. Fe(II) sorption on hematite: New insights based on spectroscopic measurements. *Environ. Sci. Technol.* **2007**, *41*, 471–477.
- (11) Peretyazhko, T.; Zachara, J. M.; Heald, S. M.; Jeon, B. H.; Kukkadapu, R. K.; Liu, C.; Moore, D.; Resch, C. T. Heterogeneous reduction of Tc(VII) by Fe(II) at the solid–water interface. *Geochim. Cosmochim. Acta* **2008**, *72*, 1521–1539.
- (12) Pedersen, H. D.; Postma, D.; Jakobsen, R.; Larsen, O. Fast transformation of iron oxyhydroxides by the catalytic action of aqueous Fe(II). *Geochim. Cosmochim. Acta* **2005**, *69*, 3967–3977.
- (13) Hansel, C. M.; Benner, S. G.; Fendorf, S. Competing Fe(II)-induced mineralization pathways of ferrihydrite. *Environ. Sci. Technol.* **2005**, *39*, 7147–7153.
- (14) Tronc, E.; Belleville, P.; Jolivet, J. P.; Livage, J. Transformation of ferric hydroxide into spinel by Fe(II) adsorption. *Langmuir* **1992**, *8*, 313–319.
- (15) Tamaura, Y.; Ito, K.; Katsura, T. Transformation of gamma-FeO(OH) to Fe₃O₄ by adsorption of iron(II) ion on gamma-FeO(OH). *J. Chem. Soc., Dalton Trans.* **1983**, 189, 194.
- (16) Pecher, K.; Haderlein, S. B.; Schwarzenbach, R. P. Reduction of polyhalogenated methanes by surface-bound Fe(II) in aqueous suspensions of iron oxides. *Environ. Sci. Technol.* **2002**, *36*, 1734–1741.
- (17) Cwiertny, D. M.; Handler, R. M.; Schaefer, M. V.; Grassian, V. H.; Scherer, M. M. Interpreting nanoscale size-effects in aggregated Fe-oxide suspensions: reaction of Fe(II) with goethite. *Geochim. Cosmochim. Acta* **2008**, *72*, 1365–1380.
- (18) Beard, B. L.; Johnson, C. M. High precision iron isotope measurements of terrestrial and lunar materials. *Geochim. Cosmochim. Acta* **1999**, *63*, 1653–1660.
- (19) Beard, B. L.; Johnson, C. M.; Skulan, J. L.; Nealson, K. H.; Cox, L.; Sun, H. Application of Fe isotopes to tracing the geochemical and biological cycling of Fe. *Chem. Geol.* **2003**, *195*, 87–117.
- (20) Crosby, H. A.; Johnson, C. M.; Roden, E. E.; Beard, B. L. Coupled Fe(II)–Fe(III) electron and atom exchange as a mechanism for Fe isotope fractionation during dissimilatory iron oxide reduction. *Environ. Sci. Technol.* **2005**, *39*, 6698–6704.
- (21) Beard, B. L.; Johnson, C. M. Fe isotope variations in the modern and ancient earth and other planetary bodies. *Rev. Mineral. Geochem.* **2004**, *55*, 319–357.
- (22) Bullen, T. D.; White, A. F.; Childs, C. W.; Vivit, D. V.; Schulz, M. S. Demonstration of significant abiotic iron isotope fractionation in nature. *Geology* **2001**, *29*, 699–702.
- (23) Jang, J. H.; Mathur, R.; Liermann, L. J.; Ruebush, S.; Brantley, S. L. An iron isotope signature related to electron transfer between aqueous ferrous iron and goethite. *Chem. Geol.* **2008**, *250*, 40–48.
- (24) Icopini, G. A.; Anbar, A. D.; Ruebush, S. S.; Tien, M.; Brantley, S. L. Iron isotope fractionation during microbial reduction of iron: The importance of adsorption. *Geology* **2004**, *32*, 205–208.
- (25) Teutsch, N.; von Gunten, U.; Porcelli, D.; Cirpka, O. A.; Halliday, A. N. Adsorption as a cause for iron isotope fractionation in reduced groundwater. *Geochim. Cosmochim. Acta* **2005**, *69*, 4175–4185.
- (26) Crosby, H. A.; Roden, E. E.; Johnson, C. M.; Beard, B. L. The mechanisms of iron isotope fractionation produced during dissimilatory Fe(III) reduction by *Shewanella putrefaciens* and *Geobacter sulfurreducens*. *Geobiology* **2007**, *5*, 169–189.
- (27) Skulan, J. L.; Beard, B. L.; Johnson, C. M. Kinetic and equilibrium Fe isotope fractionation between aqueous Fe(III) and hematite. *Geochim. Cosmochim. Acta* **2002**, *66*, 2995–3015.
- (28) Poulson, R. L.; Johnson, C. M.; Beard, B. L. Iron isotope exchange kinetics at the nanoparticulate ferrihydrite surface. *Am. Mineral.* **2005**, *90*, 758–763.
- (29) Welch, S. A.; Beard, B. L.; Johnson, C. M.; Braterman, P. S. Kinetic and equilibrium Fe isotope fractionation between aqueous Fe(II) and Fe(III). *Geochim. Cosmochim. Acta* **2003**, *67*, 4231–4250.
- (30) Shahar, A.; Young, E. D.; Manning, C. E. Equilibrium high-temperature Fe isotope fractionation between fayalite and magnetite: An experimental calibration. *Earth Planet. Sci. Lett.* **2008**, *268*, 330–338.
- (31) Silverman, J.; Dodson, R. W. The exchange reaction between the 2 oxidation states of iron in acid solution. *J. Phys. Chem.* **1952**, *56*, 846–852.
- (32) Campion, R. J.; Sutin, N.; Conocchioli, T. J. Inner-sphere activated complex for electron exchange of iron(II) + monochloro complex of iron(III). *J. Am. Chem. Soc.* **1964**, *86*, 4591–4594.
- (33) Tamura, H.; Goto, K.; Yotsuyan, T.; Nagayama, M. Spectrophotometric determination of iron(II) with 1,10-phenanthroline in presence of large amounts of iron(III). *Talanta* **1974**, *21*, 314–318.
- (34) Dixit, S.; Hering, J. G. Sorption of Fe(II) and As(III) on goethite in single- and dual-sorbate systems. *Chem. Geol.* **2006**, *228*, 6–15.
- (35) Sabioni, A. C. S.; Huntz, A. M.; Daniel, A.; Macedo, W. A. A. Measurement of iron self-diffusion in hematite single crystals by secondary ion-mass spectrometry (SIMS) and comparison with cation self-diffusion in corundum-structure oxides. *Philos. Mag.* **2005**, *85*, 3643–3658.
- (36) Freer, R.; Hauptman, Z. Experimental study of magnetite–titanomagnetite interdiffusion. *Phys. Earth Planet. Inter.* **1978**, *16*, 223–231.
- (37) Atkinson, A.; Taylor, R. I. Diffusion of ⁵⁵Fe in Fe₂O₃ single-crystals. *J. Phys. Chem. Solids* **1985**, *46*, 469–475.
- (38) Bruemmer, G. W.; Gerth, J.; Tiller, K. G. Reaction kinetics of the adsorption and desorption of nickel, zinc and cadmium by goethite. I. adsorption and diffusion of metals. *J. Soil Sci.* **1988**, *39*, 37–52.
- (39) Mikutta, C.; Lang, F.; Kaupenjohann, M. Citrate impairs the micropore diffusion of phosphate into pure and C-coated goethite. *Geochim. Cosmochim. Acta* **2006**, *70*, 595–607.
- (40) Fischer, L.; Brummer, G. W.; Barrow, N. J. Observations and modelling of the reactions of 10 metals with goethite: adsorption and diffusion processes. *Eur. J. Soil Sci.* **2007**, *58*, 1304–1315.
- (41) Yanina, S. V.; Rosso, K. M. Linked reactivity at mineral–water interfaces through bulk crystal conduction. *Science* **2008**, *320*, 218–222.
- (42) Guskos, N.; Papadopoulos, G. J.; Likodimos, V.; Patapis, S.; Yarmis, D.; Przepiera, A.; Przepiera, K.; Majszczyk, J.; Typek, J.; Wabia, M.; Aidinis, K.; Drazek, Z. Photoacoustic, EPR and electrical conductivity investigations of three synthetic mineral pigments: hematite, goethite and magnetite. *Mater. Res. Bull.* **2002**, *37*, 1051–1061.
- (43) Weidler, P. G.; Hug, S. J.; Wetche, T. P.; Hiemstra, T. Determination of growth rates of (100) and (110) faces of synthetic goethite by scanning force microscopy. *Geochim. Cosmochim. Acta* **1998**, *62*, 3407–3412.
- (44) Chun, C. L.; Penn, R. L.; Arnold, W. A. Kinetic and microscopic studies of reductive transformations of organic contaminants on goethite. *Environ. Sci. Technol.* **2006**, *40*, 3299–3304.
- (45) Larsen, F.; Postma, D. Nickel mobilization in a groundwater well field: Release by pyrite oxidation and desorption from manganese oxides. *Environ. Sci. Technol.* **1997**, *31*, 2589–2595.
- (46) Lack, J. G.; Chaudhuri, S. K.; Kelly, S. D.; Kemner, K. M.; O'Connor, S. M.; Coates, J. D. Immobilization of radionuclides and heavy metals through anaerobic bio-oxidation of Fe(II). *Appl. Environ. Microbiol.* **2002**, *68*, 2704–2710.

ES802402M